

See discussions, stats, and author profiles for this publication at: <https://www.researchgate.net/publication/222093029>

# Crystal Engineering of an Anti-HIV Drug Based on the Recognition of Assembling Molecular Frameworks

ARTICLE *in* CRYSTAL GROWTH & DESIGN · DECEMBER 2009

Impact Factor: 4.89 · DOI: 10.1021/cg900790f

---

CITATIONS

23

---

READS

21

## 4 AUTHORS, INCLUDING:



[Antonio Carlos Doriguetto](#)  
Universidade Federal de Alfenas  
119 PUBLICATIONS 894 CITATIONS

[SEE PROFILE](#)



[Javier Ellena](#)  
University of São Paulo  
410 PUBLICATIONS 2,670 CITATIONS

[SEE PROFILE](#)

# Crystal Engineering of an Anti-HIV Drug Based on the Recognition of Assembling Molecular Frameworks

Felipe T. Martins,<sup>†</sup> Nikolas Paparidis,<sup>†</sup> Antônio C. Doriguetto,<sup>‡</sup> and Javier Ellena<sup>\*,†</sup>

<sup>†</sup>Instituto de Física de São Carlos, Universidade de São Paulo, CP 369, 13560-970, São Carlos, SP, Brazil and <sup>‡</sup>Departamento de Ciências Exatas, Universidade Federal de Alfenas, Rua Gabriel Monteiro da Silva 700, 37130-000, Alfenas, MG, Brazil

Received July 10, 2009; Revised Manuscript Received October 28, 2009

**ABSTRACT:** A rational strategy was employed for design of an orthorhombic structure of lamivudine with maleic acid. On the basis of the lamivudine saccharinate structure reported in the literature, maleic acid was chosen to synthesize a salt with the anti-HIV drug because of the structural similarities between the salt formers. Maleic acid has an acid-ionization constant of the first proton and an arrangement of their hydrogen bonding functionalities similar to those of saccharin. Likewise, there is a saccharin-like conformational rigidity in maleic acid because of the hydrogen-bonded ring formation and the Z-configuration around the C=C double bond. As was conceivably predicted, lamivudine maleate assembles into a structure whose intermolecular architecture is related to that of saccharinate salt of the drug. Therefore, a molecular framework responsible for crystal assembly into a lamivudine saccharinate-like structure could be recognized in the salt formers. Furthermore, structural correlations and structure–solubility relationships were established for lamivudine maleate and saccharinate. Although there is a same molecular framework in maleic acid and saccharin, these salt formers are structurally different in some aspects. When compared to saccharin, neither out-of-plane SO<sub>2</sub> oxygens nor a benzene group occur in maleic acid. Both features could be related to higher solubility of lamivudine maleate. Here, we also anticipate that multicomponent molecular crystals of lamivudine with other salt formers possessing the molecular framework responsible for crystal assembly can be engineered successfully.

## Introduction

The solid state properties of an active pharmaceutical ingredient (API) should be understood because they are directly related to drug performance. Among all physical and chemical properties dependent on the crystalline or amorphous phase of a drug into a pharmaceutical solid dosage form, stability and solubility are those most investigated because they profoundly impact in bioavailability of a drug.<sup>1</sup> The establishment of relationships between solid-state properties and crystal structures is not easy. Most molecular structures do not exhibit similarities enough to correlate them with physical and chemical behaviors. Even though few significant advances in this sense have been made, improvements of API solid state property are achieved by crystal engineering.<sup>2</sup> Salts are particularly interesting to obtain solid-phase variants of an API with better functional characteristics.<sup>3,4</sup> Beyond low costs of production, some advantages in synthesizing API salts include practical preparation procedures, higher yield, reproducibility, and purity.<sup>5,6</sup>

Recently, multicomponent molecular crystals have been widely screened for several classes of APIs,<sup>6,7</sup> including the anti-HIV drugs.<sup>8,9</sup> The anti-HIV APIs are classified into three main categories according to molecular mechanism of action and chemical backbone: the nucleoside reverse transcriptase inhibitors (NRTIs), the non-nucleoside reverse transcriptase inhibitors (NNRTIs) and the protease inhibitors (PI).<sup>10</sup> Today, single-drug therapy has been changed to a multiple-drug one wherein at least one NRTI is ever present. Lamivudine ( $\beta$ -L-2',3'-dideoxy-3'-thiacytidine, 3TC) is one of the most clinically used NRTI in anti-HIV therapy,<sup>11</sup> being

marketed under the brand name EPIVIR.<sup>12</sup> Lamivudine is also used as a NRTI against hepatitis B virus.<sup>13</sup>

Structurally, lamivudine is a 2'-de oxygenated cytidine analog in which there is an isosteric replacement of the ribose 3'-methylene group by a sulfur atom. Concerning the configuration of their two chiral centers, lamivudine is the biologically active (−)-cis enantiomer, crystallizing always in non-centrosymmetric space groups. At least eight crystalline phases are reported for lamivudine: (1) form I, a 0.2-hydrate crystallizing as needles in the  $P2_12_12_1$  orthorhombic space group with four water and twenty lamivudine molecules per unit cell,<sup>14</sup> (2) form II, an anhydrous polymorph crystallizing in the tetragonal space group  $P4_32_12$  with eight molecules per unit cell,<sup>14</sup> which is the pharmaceutically preferred crystalline modification because of adequate manufacturing features of their bipyramidal single crystals,<sup>15</sup> (3) form III, a hemihydrate crystallizing in the monoclinic space group  $P2_1$  with one water and two lamivudine molecules per unit cell,<sup>16</sup> (4) a saccharinate salt crystallizing in the  $P2_12_12_1$  space group with four (lamivudine)<sup>+</sup>(saccharin)<sup>−</sup> ionic pairs per unit cell,<sup>8</sup> (5) a 3,5-dinitrosalicylate salt with two water and two neutral lamivudine molecules, two (lamivudine)<sup>+</sup> cations and two (3,5-dinitrosalicylic acid)<sup>−</sup> anions per monoclinic unit cell ( $P2_1$  space group),<sup>9</sup> (6) a cocrystal with 4-quinolinone formed by two lamivudine and two 4-quinolinone units per unit cell (monoclinic,  $P2_1$ ),<sup>9</sup> and (7) a hydrated cocrystal with zidovudine stoichiometrically comprising one lamivudine, one zidovudine and one water, in which there are two units of each species per monoclinic unit cell ( $P2_1$  space group).<sup>9</sup> As part of our crystal engineering researches, design and synthesis of lamivudine crystal modifications have been performed. Most recently, we have prepared (8) lamivudine duplex, which is a double-stranded helix self-assembled due to helical

\*To whom correspondence should be addressed. E-mail: javiere@ifsc.usp.br. Phone: +55 16 3373 8096. Fax: +55 16 3373 9881.

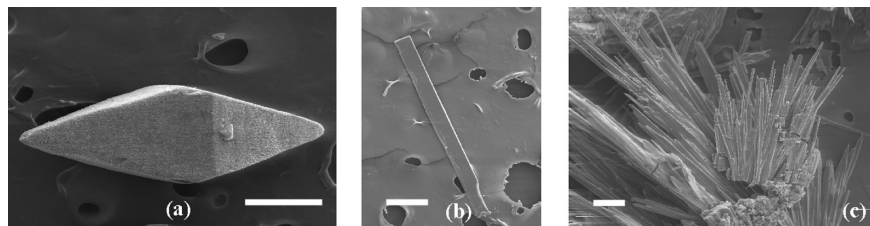


**Figure 1.** External morphology of lamivudine crystals. (a) Bipyramid of lamivudine form II isolated from the sample used for synthesis of (b) needles and (c) aggregates of lamivudine maleate. The micrographs were acquired using a scanning electron microscope (LEO 435 VP, 15 kV accelerating voltage) after the crystals were coated with colloidal gold (SCD-040 Ion Sputter Balzer device). Bar: 100  $\mu\text{m}$ .

**Table 1. Selected Crystal Data of Lamivudine Maleate and Saccharinate<sup>a</sup> and Statistic Parameters for Lamivudine Maleate Structure Determination and Refinement**

|   | lamivudine maleate  | lamivudine saccharinate <sup>a</sup>   |
|---|---|--|
| structural formula                          | (C <sub>8</sub> H <sub>12</sub> N <sub>3</sub> O <sub>3</sub> S)(C <sub>4</sub> H <sub>3</sub> O <sub>4</sub> ) | (C <sub>8</sub> H <sub>12</sub> N <sub>3</sub> O <sub>3</sub> S) (C <sub>7</sub> H <sub>4</sub> NO <sub>3</sub> S) |
| fw  | 345.33  | 412.44   |
| cryst syst                                  | orthorhombic  | orthorhombic   |
| space group                                 | P2 <sub>1</sub> 2 <sub>1</sub> 2 <sub>1</sub>   | P2 <sub>1</sub> 2 <sub>1</sub> 2 <sub>1</sub>  |
| Z   | 4   | 4  |
| T (K)                                       | 298(1)  | 100(2)   |
| unit cell dimensions                        |   |  |
| a (Å)                                       | 5.4584(3)   | 5.4130(1)  |
| b (Å)                                       | 12.8761(8)  | 12.7870(4)   |
| c (Å)                                       | 21.816(1)   | 21.6501(7)   |
| V (Å <sup>3</sup> )                         | 1533.3(2)   | 1498.53(7)   |
| calculated density (Mg/m <sup>3</sup> )     | 1.496   | 1.531  |
| absorption coefficient (mm <sup>-1</sup> )  | 0.252   | 0.258  |
| data collection and structure determination |   |  |
| $\theta$ range for data collection (deg)    | 3.22–25.53  | 3.19–25.34   |
| index ranges                                |   |  |
| h   | −6 to 6   | −6 to 6  |
| k   | −15 to 13   | −15 to 15  |
| l   | −25 to 25   | −26 to 24  |
| data collected                              | 5,067   | 16,112   |
| unique reflections                          | 2,808   | 2,711  |
| symmetry factor ( $R_{\text{int}}$ )        | 0.0621  | 0.1009   |
| completeness to $\theta_{\text{max}}$ (%)   | 98.6  | 98.7   |
| $F(000)$                                    | 720   | 720  |
| parameters refined                          | 223   | 223  |
| goodness-of-fit on $F^2$                    | 0.993   | 1.095  |
| final $R$ factors for $I > 2\sigma(I)$      | $R_I = 0.0473$ $wR_2 = 0.0839$  | $R_I = 0.0443$ $wR_2 = 0.1101$   |
| $R$ factors for all data                    | $RI = 0.1094$ $wR_2 = 0.1378$   | $RI = 0.0534$ $wR_2 = 0.1153$  |
| largest diff. peak/hole (e/Å <sup>3</sup> ) | 0.175/-0.220  | 0.373/-0.290   |
| absolute structure                          |   |  |
| parameter                                   | Flack   |  |
| value                                       | 0.18(14)  | −0.01(11)  |
| Friedel pairs                               | 1135  | 1109   |

<sup>a</sup>The crystal data for lamivudine saccharinate are in the literature<sup>8</sup> and they were shown for comparison purposes.

face-to-face stacking of the hydrogen-bonded (lamivudine) (lamivudine)<sup>+</sup> pairs in the presence of maleate and chloride counterions, and isopropanol and water molecules.<sup>17</sup> This noteworthy structure was present with eight neutral lamivudine molecules, eight protonated lamivudine cations, four maleate and four chloride anions, and two isopropanol and eight water molecules per unit cell (monoclinic, P2<sub>1</sub>).<sup>17</sup>

It is notable the capability of lamivudine to cocrystallize with different small molecules. Lamivudine is, without doubt, an attractive API for the comprehension of multicomponent molecular crystal formation in NRTIs. The assembly understanding of this type of molecular crystals is very difficult. Among other things, this includes a full crystal structure prediction and crystal formation control. In this study, we used a rational strategy to design a P2<sub>1</sub>2<sub>1</sub>2<sub>1</sub> orthorhombic structure of lamivudine with another organic acid. A salt of lamivudine with maleic acid was planned on the basis of lamivudine saccharinate.<sup>8</sup> Maleic acid is a dicarboxylic acid

extensively used as salt former for synthesis of molecular crystals. With APIs, its use to produce pharmaceutically desired solid state forms is pronounced.<sup>18–20</sup> A “replacing” of (saccharin)<sup>−</sup> by (maleic acid)<sup>−</sup> has successfully afforded the lamivudine maleate. Furthermore, structural correlations and structure–solubility relationships for lamivudine maleate and saccharinate were accurately established from the comparison of the crystal structures.

## Experimental Section

**Lamivudine Maleate Preparation.** Lamivudine form II was used for synthesis of lamivudine maleate. A lamivudine sample was first analyzed by single crystal and powder X-ray diffraction techniques before solution preparation. Unit cell measurements and X-ray diffractogram comparisons confirmed the authenticity of this sample. Then, an amount of 10 mg of the drug was dissolved in isopropanol (5 mL) under stirring for 5 min on a water bath (308 K). Next, this solution was allowed to cool to room temperature. In this step, maleic acid (5 mg) was then added to the solution.

The resulting mixture was shaken for 5 min at 298 K. All of the salt former was completely soluble. Needles and crystalline aggregates (Figure 1) arose on the bottom of the glass crystallizer after slow evaporation of the solution for 5 days in the dark within a crystal growth room (298 K). Some crystals were powdered and used to measure the melting point of lamivudine maleate (MS Tecnonon PFM II melting point apparatus).

**Lamivudine Maleate Structure Determination.** A well-grown single crystal ( $0.354 \times 0.061 \times 0.051 \text{ mm}^3$ ) was selected for X-ray diffraction data collecting at room (298 K) and low (100 K) temperatures. For low temperature experiment, a cold  $\text{N}_2$  gas blower cryogenic device (Oxford Cryosystem) was used. In the analyses, a Kappa-CCD diffractometer (Enraf-Nomius) was used as follows: Mo  $\text{K}\alpha$  radiation ( $\lambda = 0.71073 \text{ \AA}$ ), graphite monochromator,  $\varphi$  scans and  $\omega$  scans with  $\kappa$  offsets, and a 95 mm CCD camera on a  $\kappa$ -goniostat. The X-ray diffraction intensities were processed as follows: data acquisition and scaling with the COLLECT<sup>21</sup> and the HKL Denzo-Scalepack softwares,<sup>22</sup> no absorption correction because the absorption phenomenon was unimportant for lamivudine maleate (Table 1), solving by direct methods of phase retrieval with SHELXS-97<sup>23</sup> within the WinGX<sup>24</sup> package of softwares, refinement by full-matrix least-squares on  $\text{F}^2$  with SHELXL-97<sup>25</sup> within the WinGX,<sup>24</sup> constrained positions and fixed isotropic thermal parameters for C—H hydrogen atoms (bond lengths of 0.93, 0.97, and 0.98 Å for  $\text{C}_{\text{sp}}^2$ —H,  $\text{C}_{\text{sp}}^3$ —H in methylene groups, and  $\text{C}_{\text{sp}}^3$ —H in methine groups, respectively,  $U_{\text{iso}}(\text{H}) = 1.2U_{\text{eq}}(\text{C})$ ), localization of N—H,  $\text{N}^+—\text{H}$ , and O—H hydrogen atoms from the difference Fourier map and free refinement of their positions with fixed isotropic thermal parameters ( $U_{\text{iso}}(\text{H}) = 1.2U_{\text{eq}}(\text{N})$  or  $1.5U_{\text{eq}}(\text{O})$ ). After the refinement has been concluded, structure analysis and preparation of artworks were dealt with the MERCURY<sup>26</sup> and ORTEP-3<sup>27</sup> softwares. The crystallographic information file (CIF file) containing all crystal data (including data collection and processing details, refinement statistics, atomic coordinates, thermal parameters, molecular geometry and conformation, and excluding structure factors) were deposited with the Cambridge Structural Data Base under deposit codes CCDC 739173 and CCDC 739174 for the lamivudine maleate structures determined with the data collected at temperatures of 298 and 100 K, respectively. Free of charge, copies of these files may be solicited from The Director, CCDC, 12 Union Road, Cambridge, CB2 1EZ, UK, fax: +44123–336–033; e-mail: deposit@ccdc.cam.ac.uk or <http://www.ccdc.cam.ac.uk>.

**Lamivudine Maleate Purity.** The powder X-ray diffraction technique was used to assess the purity of crystalline lamivudine maleate. Samples of crystalline material formed on the bottom of glass crystallizer were finely ground and mounted on a sample holder (a grooved glass slide). A Rigaku Denki powder X-ray diffractometer with geometry  $\theta-\theta$  was used as follows: rotating anode X-ray source ( $\text{Cu K}\alpha$ ,  $\lambda = 1.5418 \text{ \AA}$ ), radiation generator at 50 kV and 100 mA, RINT2000 wide angle goniometer, continuous scan mode, scan axis  $\theta-2\theta$ , scan speed  $1.000^\circ/\text{min}$ , data acquisition width and range of  $0.020^\circ$  and  $7-40^\circ$  in  $2\theta$ , respectively. For comparison with the experimental diffractogram, the theoretical X-ray diffraction pattern of lamivudine maleate was simulated with the PowderCell software<sup>28</sup> by inputting the crystallographic information file for the structure determined based on room temperature X-ray diffraction data.

In addition, the lamivudine maleate purity was determined by high performance liquid chromatography (HPLC) analysis following the USP monograph for lamivudine quantification.<sup>29</sup> Prior to injection into the chromatograph, standard lamivudine (see below) and lamivudine maleate samples were dissolved in mobile phase (ammonium acetate solution (0.025 mol/L)/MeOH, 95:5 v/v) at a final concentration of 0.15 mg/mL. The HPLC analysis was performed at  $308 \pm 1 \text{ K}$  using a chromatograph (Shimadzu) equipped with a C18 column (LiChroSpher RP-18 (Merck) packed column ( $100 \times 4.6 \text{ mm i.d., } 5 \mu\text{m}$  particle size)) combined with a guard column ( $10 \times 4.6 \text{ mm i.d.)}$ ) and SPD-M10Avp diode array detector at 277 nm. The flow rate of mobile phase and the injected volume of each sample were  $1.0 \text{ mL/min}$  and  $20 \mu\text{L}$ , respectively.

**Lamivudine Maleate Solubility.** The equilibrium solubility of lamivudine maleate was measured according to the miniaturized

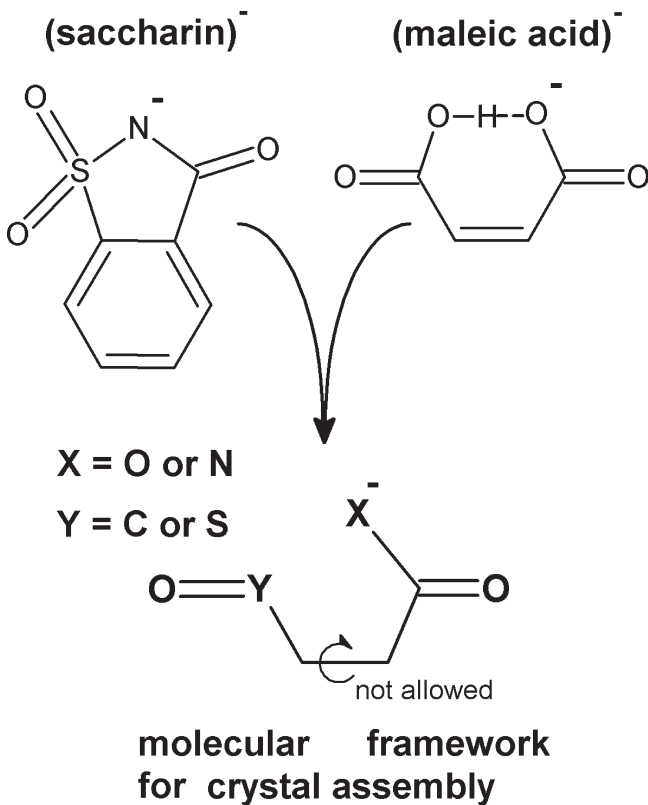


**Figure 2.** Maleic acid has a same molecular framework responsible for crystal assembly into a lamivudine saccharinate-like  $P2_12_12_1$  orthorhombic structure.

shake-flask method protocol reported in the literature.<sup>30</sup> The assays were performed in triplicate as follows: lamivudine maleate samples were added to reverse-osmosis water ( $150 \mu\text{L}$ ) at room temperature up to observation of surplus undissolved solid material (addition of about 30 mg of lamivudine maleate), shaking at 450 rpm for 24 h at temperature of  $299 \pm 2 \text{ K}$ , presence of precipitation checked every hour over a total of 8 h after the shaking beginning, filtering through a  $0.45 \mu\text{m}$  filter (Millipore) and 5000-fold dilution of filtrate aliquots ( $50 \mu\text{L}$ ), lamivudine quantification by interpolating of spectroscopic measurements from the diluted solutions in a calibration curve whose concentrations ranged from 6 to  $18 \mu\text{g/mL}$ . For this analysis, a UV–VIS spectrophotometer (Shimadzu) was used at 270 nm, and the standard solutions employed to generate the calibration curve were prepared using a standard material of lamivudine from the Instituto Nacional de Controle de Qualidade, FIOCRUZ (lamivudine purity of  $99.55 \pm 0.07 \text{ mol } \%$ , which was determined by differential scanning calorimetry according to the ASTM E928 standard specification).

## Results and Discussion

Recently, a lamivudine salt was prepared with saccharin.<sup>8</sup> On the basis of the structure of this salt, we have planned another crystalline modification of lamivudine using a rational approach for its design. First, saccharin is deprotonated in the structure because of a proton transfer from it to lamivudine. Then, a salt former with an acid-ionization constant ( $\text{pK}_a$ ) similar to that of saccharin should be intended because its deprotonation is needed for protonation of lamivudine. Second, each saccharinate fragment is bonded to two lamivudine molecules in the structure through three hydrogen bonds. At last, saccharin is conformationally rigid. As one can presume, the functional hydrogen acceptor groups of saccharinate anion are limited to some positions in the crystal. Therefore, the salt former engineered for replacing of saccharinate anion

within the orthorhombic structure should obey a conformational rigidity around the hydrogen-bonding functionalities. Incredibly, a small molecule very used in pharmaceutical processes for a long time has all these required structural features. It is maleic acid. First, the  $pK_{a1}$  of maleic acid is 1.83.<sup>31</sup> This value is almost equal than that of saccharin, ~1.8,<sup>32,33</sup> even though other studies report a  $pK_a$  value of 2.2 for saccharin.<sup>8,34</sup> Although there are differences in the saccharin  $pK_a$  values reported, which can be the result of different measurement conditions, it is right to state that the acid strength of saccharin is very similar to that for the first proton ionization of maleic acid since a  $pK_a$  value of 1.8 is reported for saccharin. Second, the carboxylate moiety of (maleic acid)<sup>-</sup> has two functional hydrogen acceptor oxygens, while the

carboxyl group has one oxygen atom able to be readily engaged in an intermolecular interaction through hydrogen bonding acceptance from lamivudine. These three oxygens of maleate are spaced as those N<sup>(-)</sup> nitrogen, C=O, and S=O oxygens of (saccharin)<sup>-</sup> (Figure 2). Similar to Z-configuration in (maleic acid)<sup>-</sup> setting the COO<sup>(-)</sup> and COOH groups in the same side relative to the C=C double bond, the CON<sup>(-)</sup> and SO<sub>2</sub> moieties of saccharinate are in a cis orientation relative to the C=C bond bridging the two fused rings. Indeed, the arrangement of the four carbons of (maleic acid)<sup>-</sup> resembles that of the C=O carbon, the two bridge carbons and the sulfur atom of (saccharin)<sup>-</sup>. Likewise, the four oxygen atoms of (maleic acid)<sup>-</sup> are analogously related to the two SO<sub>2</sub> oxygens, the C=O oxygen and the N<sup>(-)</sup> nitrogen of (saccharin)<sup>-</sup>. These structural similarities between the salt formers are illustrated in Figure 2. At last, the conformational rigidity found in saccharinate is also present in maleate because of the hydrogen-bonded ring formation and, mainly, the C=C double bond. However, two greater differences between saccharin and maleic acid are notable: the two SO<sub>2</sub> oxygens of (saccharin)<sup>-</sup> are out of the molecule plane and this salt former has a benzene tail fused to the isothiazolidinone-S,S-dioxide moiety, whereas all oxygens of (maleic acid)<sup>-</sup> are coplanar to the only four carbons comprising its acyclic chain. Fortunately, lamivudine maleate salt is obtained according to the rational design and these differences were important to establish the structure-solubility relationships.

After the synthesis, the lamivudine maleate structure was determined at room (298 K) and low (100 K) temperatures by

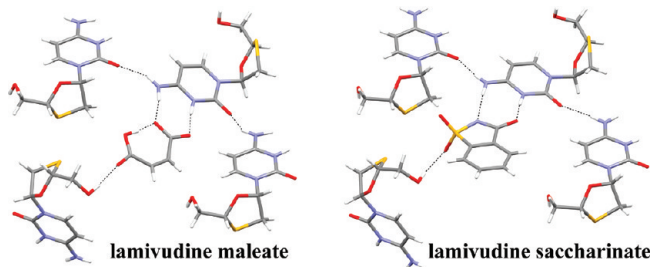


**Figure 3.** Hydrogen bonding pattern of lamivudine maleate and saccharinate.<sup>8</sup> The representation of the saccharinate salt was prepared using the VAWPIT CIF file.

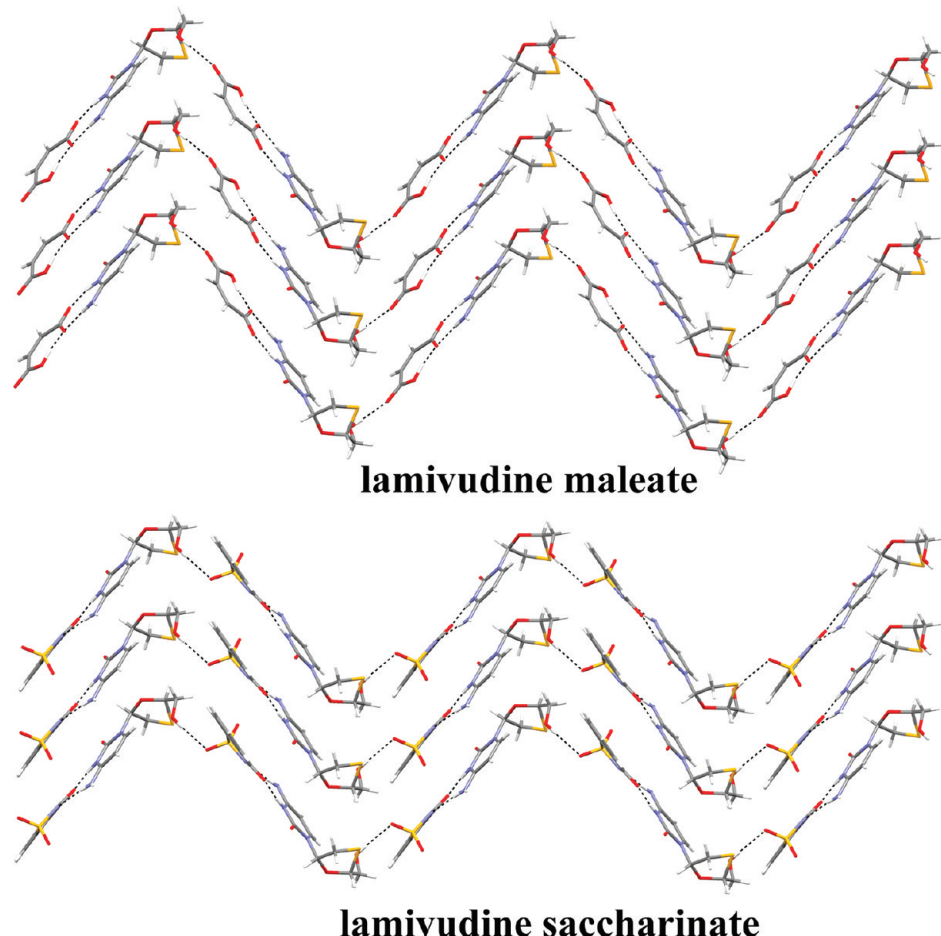


**Figure 4.** Lamivudine and salt former are alternate along the [001] direction. The drawing of the saccharinate salt was prepared using the VAWPIT CIF file.<sup>8</sup>

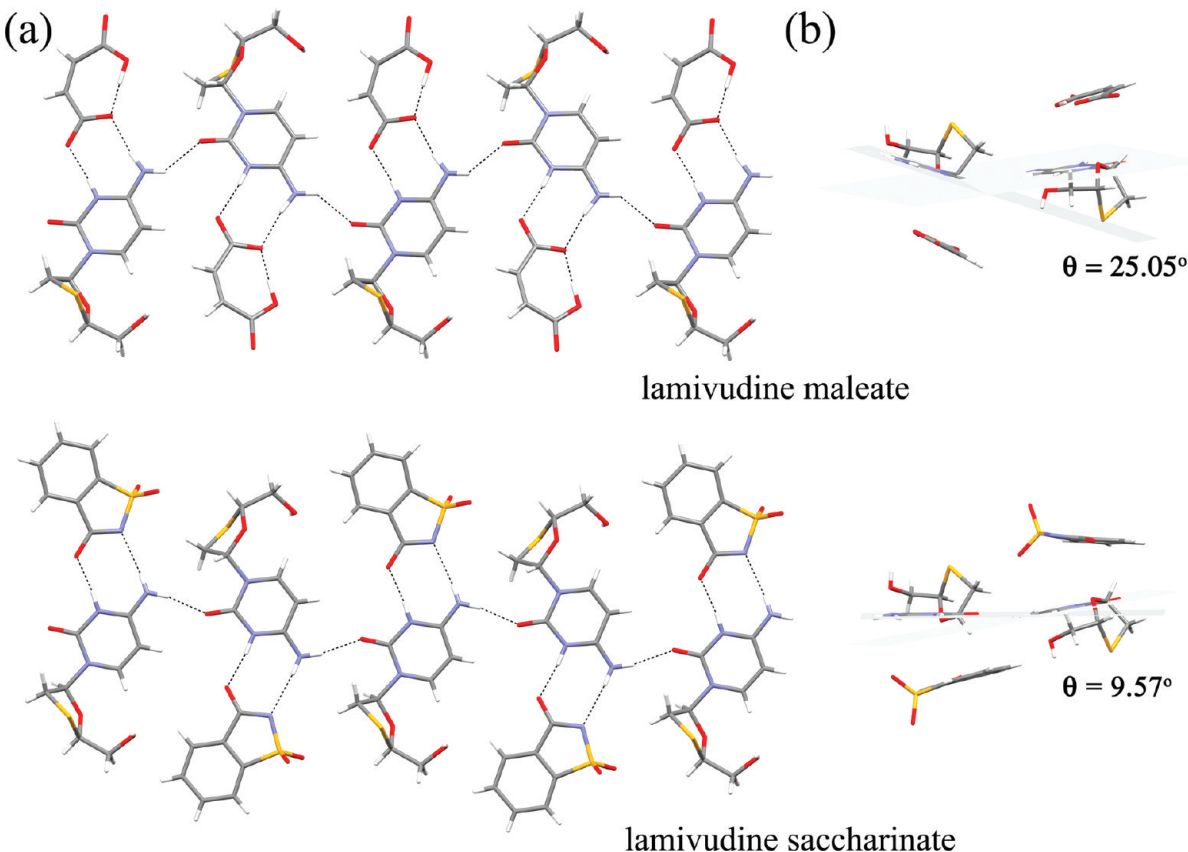


**Figure 5.** (a) The  $(\text{lamivudine})^+(\text{salt former})^-$  pairs are connected to each other along the [010] direction through hydrogen bonds between the cytosine fragments of lamivudine. (b) The least-squares planes passing through the cytosine rings of lamivudine are more aligned in the saccharinate salt than in the maleate version of the drug because packing forces drive the assembly of cytosine fragments of lamivudine and salt former molecules on a neighboring layer. The illustration of lamivudine saccharinate was prepared using VAWPIT CIF file.<sup>8</sup>

single crystal X-ray diffraction analysis. The X-ray diffraction measurements revealed that unit cell parameters and molecular assembly of lamivudine maleate do not vary significantly with the temperature in this range (Table 1). Therefore, these experiments demonstrate that no solid–solid phase transformation occurs between the evaluated temperatures.

As it was conceivably predicted, lamivudine maleate assembles into a structure whose molecular arrangement is related to that of the saccharinate salt of the drug. Furthermore, the crystallographic unit cell dimensions of lamivudine maleate are similar to the corresponding values of the saccharinate salt (Table 1). This is in agreement with the network similarity of the lamivudine salts. The  $\text{N}^{(+)}-\text{H}\cdots\text{O}=\text{C}$  and  $\text{N}-\text{H}\cdots\text{O}^--\text{C}$  hydrogen bonds involving the cytosine ring of the drug and the carboxylate group of (maleic acid)<sup>-</sup> mimic the  $\text{N}^{(+)}-\text{H}\cdots\text{O}=\text{C}$  and  $\text{N}-\text{H}\cdots\text{N}^{(-)}-\text{C}$  present in the saccharinate salt (Figure 3). The hydroxymethylene tail of lamivudine is hydrogen-bonded to (maleic acid)<sup>-</sup> through  $\text{O}-\text{H}\cdots\text{O}=\text{C}$  atoms. The carbonyl oxygen of the carboxyl group is a hydrogen acceptor of the anion in this interaction. In lamivudine maleate, this oxygen functions as one of the two  $\text{SO}_2$  oxygens of (saccharin)<sup>-</sup>, which is a hydrogen acceptor in the  $\text{O}-\text{H}\cdots\text{O}=\text{S}$  hydrogen bonding of lamivudine saccharinate (Figure 3). These aforementioned hydrogen bonds, wherein the  $\text{N}^{(+)}-\text{H}$ ,  $\text{N}-\text{H}$ , and  $\text{O}-\text{H}$  functionalities of the drug are hydrogen donors, assemble alternate molecules of  $(\text{lamivudine})^+$  and  $(\text{maleic acid})^-$  (or saccharinate) along the [001] direction, giving rise to a zigzag fashioned one-dimensional ribbon (Figure 4). As in the saccharinate salt of the

drug, there is also in the maleate salt structure a  $\text{N}-\text{H}\cdots\text{O}=\text{C}$  hydrogen bond between the cytosine rings of adjacent lamivudine molecules. These molecules are related by a  $2_1$  screw axis symmetry along the [010] direction (Figure 5a). Similar to a  $\text{S}=\text{O}$  oxygen of (saccharin)<sup>-</sup>, which is not hydrogen-bonded in the lamivudine saccharinate structure, the hydroxyl oxygen of maleate is not a hydrogen acceptor in the salt.

In the maleate and saccharinate salts, the lamivudine conformation is remarkably similar. In Figure 6, the lamivudine molecules in the maleate and saccharinate salt structures are superimposed in a capped stick fashion to illustrate the conformational similarity for drug fragments in these crystalline modifications. Here, a brief description of the most relevant conformational features of lamivudine molecule in the maleate salt is given. Because the molecular conformations of lamivudine in maleate and saccharinate salts are similar, only structural description of the drug in the novel solid state phase is presented. This lamivudine conformer was inspected from the maleate salt structure determined using X-ray diffraction data collected at low temperature. A more reliable comparison is gotten by analyzing this conformer because the lamivudine saccharinate structure was determined with data collected at 100 K.<sup>8</sup> Likewise, all values of conformational and geometrical parameters found throughout the text were measured using this structure. The non-hydrogen atoms in the asymmetric unit of lamivudine maleate (at 100 K) are represented as 50% probability thermal displacement ellipsoids in Figure 7. The opposite orientation of the carbonyl oxygen

relative to the oxathiolane ring describes an *anti* conformation of the cytosine fragment ( $C_2-N_1-C_1'-O_1'$  torsion measures  $161.4(2)^\circ$ ). The five-membered oxathiolane ring adopts a puckering conformation. The sulfur atom is at the flip point of the puckered system. It deviates from the well-fitted least-squares plane passing through the other four cyclic atoms by  $0.8415(8)$  Å (the root-mean-square deviation (rmsd) of the four fitted atoms is  $0.0431$  Å). The sulfur atom is also *cis* oriented relative to cytosine fragment ( $O_1'-C_1'-C_2'-S_3'$  dihedral angle measures  $37.2(3)^\circ$ ). This describes a conformation related to the  $C_3'$ -endo puckering mode that occurs in the canonical nucleosides. Concerning the conformation of the hydroxymethylene tail, the arrangement of the substituents around the methylene  $sp^3$ -hybridized carbon describes an axial orientation of the hydroxyl oxygen, which is also on the same side of cytosine ring relative to the oxathiolane plane ( $O_1'-C_4'-C_5'-O_5'$  torsion value is  $60.4(3)^\circ$ ).

Even though the crystal assemblies of maleate and saccharine salts of lamivudine are similar, some aspects of packing are different. The intermolecular hydrogen bonding geometry of

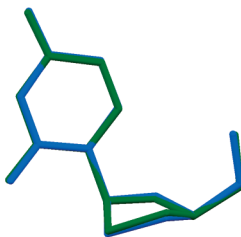


**Figure 6.** Superposition of lamivudine molecules in the maleate (green) and saccharinate (blue) salts. All hydrogen atoms were omitted for drawing clarity.

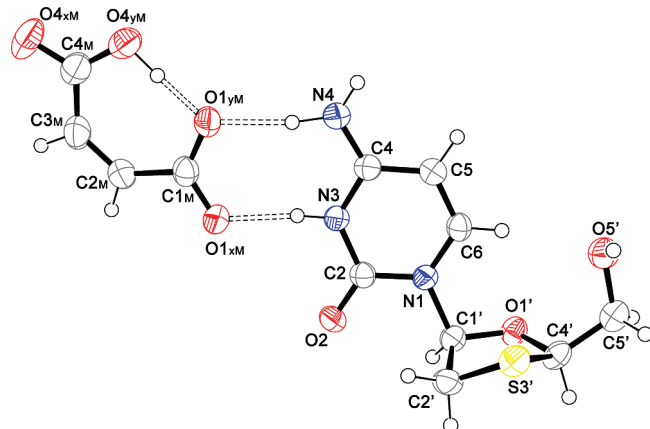


**Figure 7.** Crystallographic asymmetric unit of lamivudine maleate. Arbitrary radius spheres and 50% probability ellipsoids draw the hydrogen and non-hydrogen atoms, respectively.

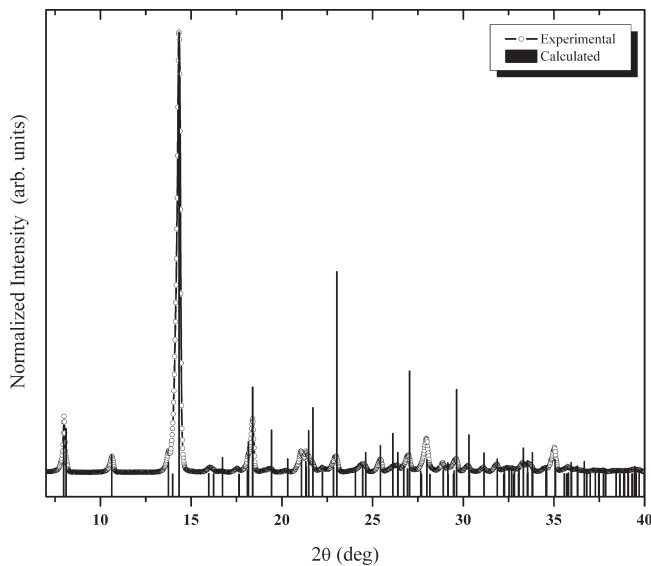


**Figure 8.** Calculated and room temperature experimental powder X-ray diffractograms of lamivudine maleate. The calculated diffractogram was simulated from the crystal structure determined at 298 K.

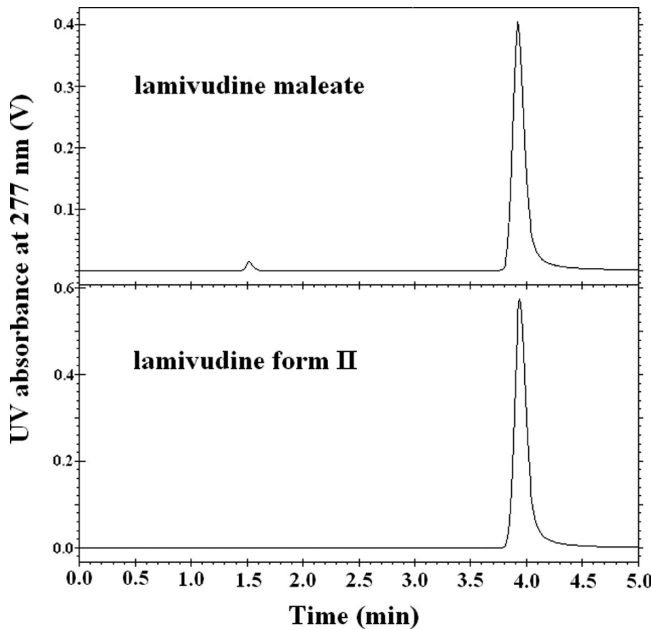


**Figure 9.** The purity of lamivudine maleate was assessed by high performance liquid chromatography (HPLC) analysis. The lamivudine form II was used as standard (see Experimental Section). The maleic acid peak could be detected in the lamivudine maleate chromatogram (retention time of  $\sim 1.5$  min).

**Table 2. Geometry of Hydrogen Bonds in Lamivudine Maleate and Lamivudine Saccharinate<sup>8</sup>**

| $D-H\cdots A$               | $H\cdots A$ (Å) |                           | $D-H$ (Å) |              | $D\cdots A$ (Å) |              | $D-H\cdots A$ (deg) |              |
|-----------------------------|-----------------|---------------------------|-----------|--------------|-----------------|--------------|---------------------|--------------|
|                             | maleate         | saccharinate <sup>d</sup> | maleate   | saccharinate | maleate         | saccharinate | maleate             | saccharinate |
| $N^{(+)}-H\cdots O$         | 0.89(4)         | 0.87(3)                   | 1.80(4)   | 1.78(3)      | 2.675(3)        | 2.644(2)     | 169(4)              | 171(2)       |
| $N-H\cdots O^{(-)}/N^{(-)}$ | 0.98(4)         | 0.81(3)                   | 1.85(3)   | 2.14(3)      | 2.822(3)        | 2.946(2)     | 171(3)              | 172(3)       |
| $N-H\cdots O^b$             | 0.87(4)         | 0.89(3)                   | 2.06(4)   | 1.96(3)      | 2.789(3)        | 2.838(2)     | 141(3)              | 167(2)       |
| $O-H\cdots O^c$             | 0.79(5)         | 0.77(3)                   | 1.90(5)   | 2.17(3)      | 2.686(3)        | 2.928(2)     | 173(5)              | 170(3)       |

<sup>a</sup> D, hydrogen donor; A, hydrogen acceptor. <sup>b</sup> Symmetry operator:  $1-x, -0.5+y, 1.5-z$ . <sup>c</sup> Symmetry operator:  $1.5-x, -y, 0.5+z$ . <sup>d</sup> Hydrogen bonding metrics for lamivudine saccharinate were obtained from VAWPIT CIF file.

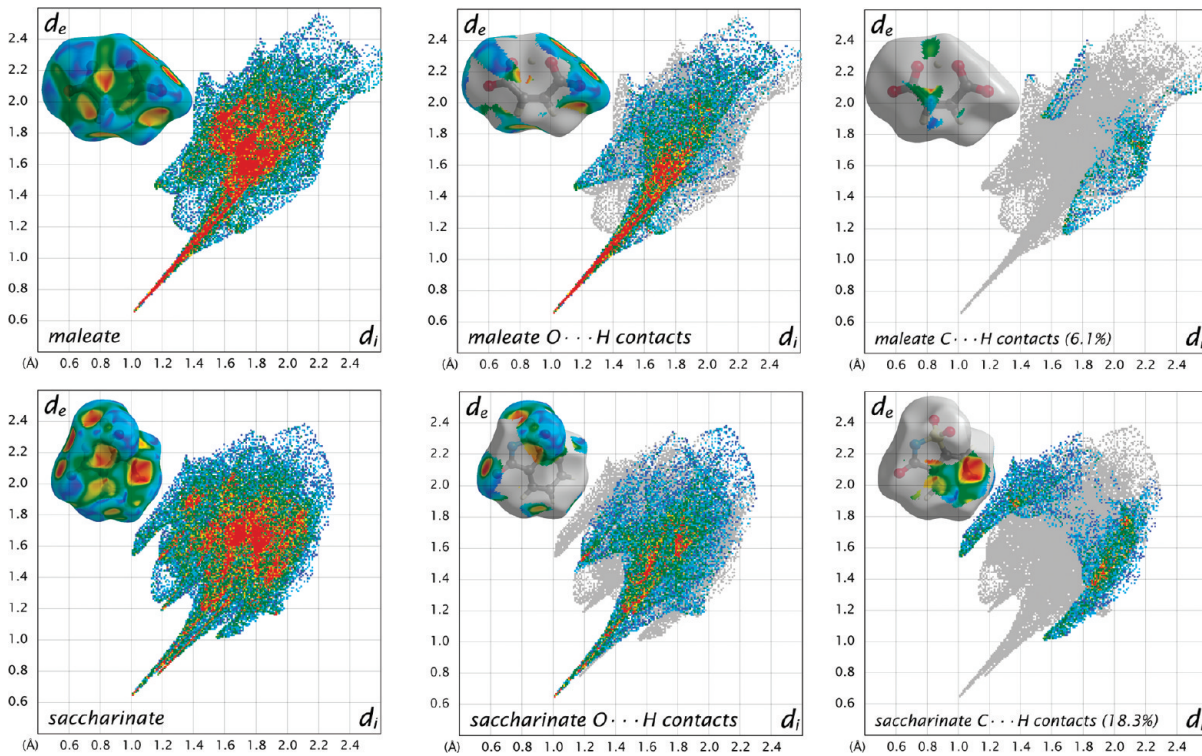


**Figure 10.** Hirshfeld surface analysis for maleate and saccharinate anions in the lamivudine salts. Points of fingerprint graphics constructed from Hirshfeld surface data are colored blue (lower proportions of the ( $d_i, d_e$ ) pair), green (intermediary frequency of the ( $d_i, d_e$ ) pair) or red (proportion of the ( $d_i, d_e$ ) pair greater than 0.1% of the surface spots). The  $d_i$  internal distance is the shortest separation from the Hirshfeld surface to an atomic nucleus of the fragment taken for surface calculation, whereas  $d_e$  is the external distance between the Hirshfeld surface and the nearest atom of a neighboring species within the crystal. Parentheses surround the percentage of the ( $d_i, d_e$ ) pairs regarding the C $\cdots$ H contacts. The Hirshfeld surface is represented as a map of shape index on the salt former molecules. The sharp spikes correspond to the hydrogen bonding acceptor groups of maleate and saccharinate anions.

lamivudine maleate and saccharinate is displayed in Table 2. The main difference in hydrogen bond metrics for the salt structures is in the directionality of a N—H $\cdots$ O=C contact between the cytosine cores of lamivudine. The angle value of this hydrogen bonding in lamivudine maleate is very less than the corresponding value in the saccharinate salt. These measurements change by  $\sim 26^\circ$  (bold in Table 2). Such difference is related to the lesser alignment of cytosine rings in lamivudine maleate. In this salt, the mean planes passing through the cytosine rings of lamivudine molecules connected through N—H $\cdots$ O=C atoms are tilted by  $25.05(8)^\circ$ , whereas the corresponding bend between cytosine rings in lamivudine saccharinate is  $9.57(6)^\circ$  (Figure 5b). The alignment of cytosine planes in lamivudine saccharinate is a consequence of packing forces driving the assembly of the cytosine moieties and the bulkier structure of saccharinate on a neighboring layer. One of the two out-of-plane SO<sub>2</sub> oxygens also contributes to align the pyrimidinone bases in the former structure (Figure 5b). Therefore, the cytosine planes are more bent in lamivudine maleate than in the saccharinate salt structure.

Lamivudine and maleic acid were stoichiometrically crystallized together. The 1:1 stoichiometry and the crystalline purity of this salt were verified by powder X-ray diffraction and high performance liquid chromatography (HPLC) analyses. All peaks in the experimental X-ray diffractogram of powdered samples of crystalline material formed after the crystallization procedure (see Experimental Section) (Figure 8) overlaid to those observed in the simulated X-ray diffractogram from the single crystal structure of lamivudine maleate (data collection at 298 K). Therefore, we can conclude that the

powdered lamivudine maleate product has no extra crystalline phase. Also, since no broad hump from amorphous material was observed the powdered sample is completely crystalline. Moreover, preferred orientation effects were observed in the experimental powder X-ray diffraction pattern of lamivudine maleate. The X-ray diffraction intensities in the simulated and experimental diffractograms were different because of the most intense Bragg (0 2 1) reflection preferred orientation. One species of (lamivudine)<sup>+</sup> and one of (maleic acid)<sup>-</sup> are present in the crystallographic asymmetric unit of the determined structures. The proposed stoichiometry of the crystal is in agreement with refined unit cell content, which is strengthened by HPLC analysis (Figure 9). From the chromatographic experiment, lamivudine was found to be in  $0.699 \pm 0.006$  g/g of crystalline material. This experimental finding is in accordance with the calculated value for an equimolar stoichiometry of pure lamivudine maleate crystals. This predicted value is 0.667 mg of lamivudine/g of lamivudine maleate. Adopting an equimolarity of the maleate salt, a relative purity of  $104.8 \pm 0.8\%$  was found for the obtained crystalline material.

The thermodynamic solubility of lamivudine maleate was evaluated in this study. The structure-solubility relationships were established for the lamivudine salts based on the maleate and saccharinate salt structures. The meaningful determination of correlations between crystal structure and solid state properties has been a challenge in the crystal engineering research field.<sup>8</sup> Progress on the understanding of the main factors influencing salt dissolution has been succeeded.<sup>35</sup> For instance, it is known that the water solubility of six amine salts

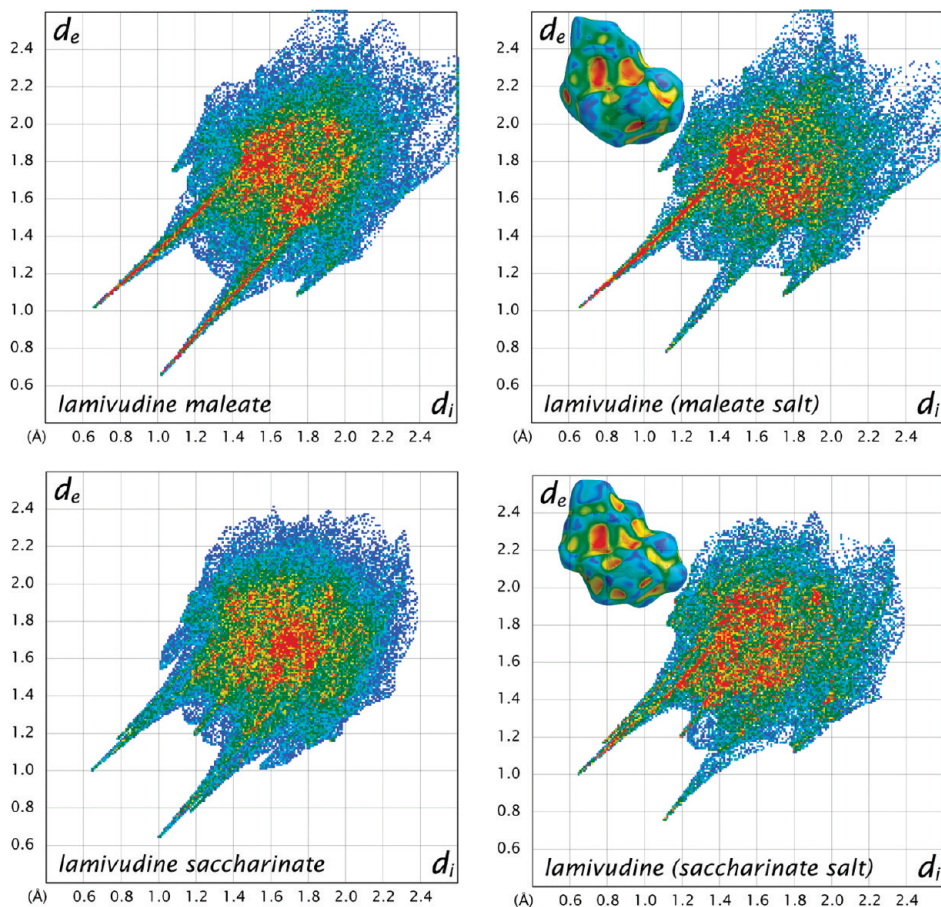


**Figure 11.** Hirshfeld surface analysis for the lamivudine salts and  $(\text{lamivudine})^+$  cations. Point coloring scheme of the fingerprint graphics is detailed in Figure 10 caption. Maps of shape index are on the Hirshfeld surface calculated for the lamivudine fragments in the salts. Prominent sharp spikes of plots refer to classical hydrogen bonds. The upper and lower spikes are related to hydrogen bonding donor and acceptor groups, respectively.

of the anti-inflammatory drug flurbiprofen is strongly related to melting point, while no correlation between solubility and amine cation hydrophilicity is observed.<sup>36</sup> Recently, the anti-convulsant drug lamotrigine was crystallized with some dicarboxylic acids (succinic acid, fumaric acid, DL-tartaric acid) and saccharin.<sup>37</sup> In this study, the water solubility of the salts was only associated with the solubility of salt formers, although the solubility of some dicarboxylate salts could be rationalized on the basis of crystal packing features because they were isostructural. Despite the lamotrigine saccharinate crystals were not suitable for single-crystal X-ray diffraction analysis, its structure is expected to be different from that of the dicarboxylate salts.<sup>37</sup> In agreement with our results in which *Z*-configured maleic acid forms a salt with lamivudine whose structure is resembled that of the saccharinate salt of the drug, *E*-configuration in fumaric acid and the higher flexibility of succinic acid and tartaric acid that configures a trans conformation of the carboxylate groups with respect to the central carbon chain are responsible for different positioning of their hydrogen bonding functionalities than that of saccharinate anion. Therefore, this explains the differences between lamotrigine saccharinate and crystal structures of dicarboxylate salts of the drug. Regarding the lamivudine salts, this paper means an advance in an understanding of their structure-solubility correlations. The lamivudine saccharinate solubility of 10.56 mg/mL is reported in the literature.<sup>8</sup> The free base of the drug, which is incorporated into clinical formulations, is more soluble than lamivudine

saccharinate. Its solubility is about 70 mg/mL. Therefore, the solubility of lamivudine maleate was expected to be less than that of the pharmaceutically preferred solid phase of lamivudine (form II) because the maleate salt was structurally planned from the saccharinate salt of lamivudine. The crystal lattice stability of lamivudine maleate and saccharinate should be comparable. In agreement with the solubility behavior prediction, we have found a solubility value of  $45 \pm 3$  mg/mL for lamivudine maleate. Interestingly, the lamivudine maleate is more soluble than the saccharinate version of the drug. Furthermore, melting temperatures of the maleate and saccharinate versions of the drug indicate that the lattice energy of the lamivudine salts can be correlated to solubility. A melting point of 144 °C was measured for lamivudine maleate, while the melting temperature of 182.3 is reported for lamivudine saccharinate.<sup>8</sup> In this way, a lower melting point of lamivudine maleate is in agreement with its higher solubility when compared to lamivudine saccharinate. This reveals that the crystal lattice energies of the lamivudine salts play a relevant role in their solubilities. Despite lamivudine maleate and lamivudine saccharinate are structurally similar, lipophilicity and water solubility of the anions are quite different. The anion (*saccharin*)<sup>-</sup> has a benzene core fused to the isothiazolidinone-S,S-dioxide moiety. So, lipophilicity of (*saccharin*)<sup>-</sup> is higher than that of (*maleic acid*)<sup>-</sup>. Aqueous solubility values reflect the lipophilic character of the anions. Saccharin solubility is 4 mg/mL in water, while the corresponding measurement for maleic acid is 441 mg/mL.<sup>38</sup>

This notable difference in water solubility of the salt formers indicates that their ionic forms should also have different solvation energies. Therefore, solvation thermodynamics also plays a significant role in the solubility of the lamivudine salts because of different properties of the anions. Solubility behavior of lamivudine maleate and lamivudine saccharinate can be also understood as a consequence of the unfavorable directionality of the N—H $\cdots$ O=C hydrogen bond between the cytosine rings of lamivudine in the maleate salt. This decreases the stabilization of lamivudine maleate when compared to the saccharinate salt. Therefore, the higher solubility of lamivudine maleate is rationalized. It is important to highlight that the directionality gain in lamivudine saccharinate is from the alignment of cytosine planes caused by packing driven forces. Indeed, the comparison between maleic acid and saccharin reveals that other structural features of (saccharin) $^-$  are related to lower solubility of its salt with lamivudine. Once three suitably spaced hydrogen bonding acceptors are present in a salt former, the  $P2_12_12_1$  orthorhombic structure of lamivudine is assembled because hydrogen bonds can be formed in the structures. Although these molecular motifs are required, further groups can be attached to the crystallophore (claimed here as being a molecular framework of a salt former or cocrystallizing agent owning the least structural requisites responsible for the self-assembly of a structurally defined multicomponent molecular crystal, in analogy to pharmacophore definition in medicinal chemistry). Unlike maleic acid, saccharin has a fused benzene ring that helps stabilize the lamivudine saccharinate structure through weak contacts other than classical hydrogen bonds. There are interactions of the C—H $\cdots$ C type between the benzene portions of (saccharin) $^-$  in the lamivudine salt. Contacts of this type are present with a considerable proportion of the two-dimensional Hirshfeld fingerprint plot<sup>39</sup> for (saccharin) $^-$  in the API salt, whereas they have a minor importance in the corresponding graphic for (maleic acid) $^-$  (Figure 10). These contacts contribute to support the differences in lattice energy of the lamivudine salts, which helps rationalize the higher lattice energy of lamivudine saccharinate and, therefore, its lower solubility with respect to lamivudine maleate. In this way, weak contacts play a fine-tuning role in the lamivudine salt solubilities since strong hydrogen bonds are primarily responsible for the crystal assembly. Furthermore, intermolecular contact patterns of the drug are resembled in these salts. In Figure 11, the Hirshfeld surface analysis for (lamivudine) $^+$  cations in both salt structures graphically illustrates the previous observation. The fingerprint graphics constructed from the Hirshfeld surface data for lamivudine fragments in maleate and saccharinate salts are practically identical. Hirshfeld surface graphically describes assembling patterns because this crystal property is calculated from intermolecular interactions present in crystal structures. At last, the hydrophobicity of (saccharin) $^-$  is increased when compared to (maleic acid) $^-$ , rationalizing the lower solubility of lamivudine saccharinate because its solvation in aqueous medium is less favorable than that of lamivudine maleate.

## Conclusion

The understanding of multicomponent molecular crystal assembly has been a challenge in the crystal engineering research field for a long time. Complete crystal structure prediction and crystal formation control are very difficult. In this sense, this paper means important advances because an

API salt was successfully designed using a rational approach for the salt former choice. Chemical aspects of salt formers and crystal assembly features were taken into account for selection of maleic acid to assemble into a predicted  $P2_12_12_1$  orthorhombic structure with lamivudine. Acid-ionization constant, arrangement of hydrogen bonding functionalities and conformational features were considered for selection of the salt former. A rationally designed crystal synthesis and the establishment of structure—property relationships are some advantages of this strategy. The unfavorable directionality of hydrogen bonds could be related to an increased solubility of lamivudine maleate when compared to the saccharinate version of the drug. Here, we anticipate that multicomponent molecular crystals comprising lamivudine and other salt formers possessing the molecular framework responsible for crystal assembly can be engineered successfully. At last, the inventive and nonobvious characters of rationally synthesized API salts surely will lead to an easier legal procedure for protection of intellectual property rights.

**Acknowledgment.** We thank Dr. Altivo Pitaluga Jr. (Fundação Oswaldo Cruz, FIOCRUZ, Manguinhos, Rio de Janeiro, Brazil) for the gift of lamivudine samples. Rudy Bonfilio and Prof. Ph.D. Magali B. de Araújo from the Centro de Equivalência Farmacêutica (Núcleo de Controle de Qualidade de Fármacos e Medicamentos, Universidade Federal de Alfenas, CEFAR-NCQ/UNIFAL-MG) are also acknowledged for assistance in high performance liquid chromatography analysis and solubility measurements. We thank the Brazilian Research Council CNPq (Conselho Nacional de Desenvolvimento Científico e Tecnológico) and FAPESP (Fundação de Amparo à Pesquisa do Estado de São Paulo, Grant 2007/07185-5) for research fellowships (A.C.D., J.E., and F.T.M.). We also thank FAPEMIG (Fundação de Amparo à Pesquisa do Estado de Minas Gerais, APQ-2011-5.02/07, APQ-6010-5.02/07, APQ-02685-09) and CAPES (Coordenação de Aperfeiçoamento de Pessoal de Nível Superior, Grant PNPD2008) for financial support.

**Supporting Information Available:** Crystallographic information in CIF format. This material is available free of charge via the Internet at <http://pubs.acs.org>.

## References

- (1) Lu, J.; Wang, X.-J.; Yang, X.; Ching, C.-B. *Cryst. Growth Des.* **2007**, *7*, 1590–1598.
- (2) Grant, D. J. W. In *Polymorphism in Pharmaceutical Solids*; Brittain, H. G., Ed.; Dekker: New York, 1999; Vol. 95, pp 1–33.
- (3) Bond, A. D. *CrystEngComm* **2007**, *9*, 833–834.
- (4) Lara-Ochoa, F.; Espinosa-Pérez, G. *Cryst. Growth Des.* **2007**, *7*, 1213–1215.
- (5) Miroshnyk, I.; Mirza, S.; Sandlert, N. *Expert Opin. Drug Delivery* **2009**, *6*, 333–341.
- (6) Almarsson, Ö.; Zaworotko, M. *J. Chem. Commun.* **2004**, 1889–1896.
- (7) Cheney, M. L.; McManus, G. J.; Perman, J. A.; Wang, Z.; Zaworotko, M. *J. Cryst. Growth Des.* **2007**, *7*, 616–617.
- (8) Banerjee, R.; Bhatt, P. M.; Ravindra, N. V.; Desiraju, G. R. *Cryst. Growth Des.* **2005**, *5*, 2299–2309.
- (9) Bhatt, P. M.; Azim, Y.; Thakur, T. S.; Desiraju, G. R. *Cryst. Growth Des.* **2009**, *9*, 951–957.
- (10) Greene, W. C.; Debyser, Z.; Ikeda, Y.; Freed, E. O.; Stephens, E.; Yonemoto, W.; Buckheit, R. W.; Este, J. A.; Cihlar, T. *Antiviral Res.* **2008**, *80*, 251–265.
- (11) Coates, J. A.; Cammack, N.; Jenkinson, H. J.; Mutton, I. M.; Pearson, B. A.; Storer, R.; Cameron, J. M.; Penn, C. R. *Antimicrob. Agents Chemother.* **1992**, *36*, 202–205.
- (12) Belleau, B.; Nguyen-Ba, N. U.S. Patent US5047407, October 9, 1991.

- (13) Chang, C. N.; Skalskiv, V.; Zhou, J. H.; Cheng, Y. C. *J. Biol. Chem.* **1992**, *267*, 22414–22420.
- (14) Harris, R. K.; Yeung, R. R.; Lamont, R. B.; Lancaster, R. W.; Lynn, S. M.; Staniforth, S. E. *J. Chem. Soc., Perkin Trans. 2* **1997**, 2653–2659.
- (15) Jozwiakowski, M. J.; Nguyen, N. T.; Sisco, J. M.; Spancake, C. W. *J. Pharm. Sci.* **1996**, *85*, 193–199.
- (16) Singh, G. P.; Srivastava, D.; Saini, M. B.; Upadhyay, P. R. Int. Patent WO2007119248, October 25, 2007.
- (17) Martins, F. T.; Doriguetto, A. C.; Ellena, J. *Cryst. Growth Des.* [Online early access]. DOI: 10.1021/cg901103r. Published Online October 15, 2009.
- (18) Takahashi, S.; Inoue, K.; Yanagida, Y.; Ohashi, T.; Watanabe, K. European Patent EP215335, March 25, 1987.
- (19) Eswaraiah, S.; Reddy, G. M.; Reddy, J. M.; Rambabu, K. V.; Bhaskar, B. V. U. S. Patent US2007004783, January 4, 2007.
- (20) Hu, M.; Paliwal, S.; Shih, N.; Guenter, F.; Mergelsberg, I. International Patent WO2007114922, October 11, 2007.
- (21) COLLECT Data Collection Software; Nonius: Delft, The Netherlands, 1998.
- (22) Otwinowski, Z.; Minor, W. In *Methods in Enzymology: Macromolecular Crystallography, Part A*; Carter, C. W., Jr., Sweet, R. M., Eds.; Academic Press: New York, 1997; Vol. 276, pp 307–326.
- (23) Sheldrick, G. M. *SHELXS-97: Program for Crystal Structure Resolution*; University of Göttingen: Göttingen, Germany, 1997.
- (24) Farrugia, L. J. *J. Appl. Crystallogr.* **1999**, *32*, 837–838.
- (25) Sheldrick, G. M. *SHELXL-97: Program for Crystal Structure Analysis*; University of Göttingen: Göttingen, Germany, 1997.
- (26) Bruno, I. J.; Cole, J. C.; Edgington, P. R.; Kessler, M. K.; Macrae, C. F.; McCabe, P.; Pearson, J.; Taylor, R. *Acta Crystallogr., Sect. B* **2002**, *58*, 389–397.
- (27) Farrugia, L. J. *J. Appl. Crystallogr.* **1997**, *30*, 565.
- (28) Kraus, W.; Nolze, G. *PowderCell for Windows*, version 2.3; Federal Institute for Materials Research and Testing: Berlin, Germany, 1999.
- (29) *The United States Pharmacopeia XXXI and National Formulary XXVI*; The United States Pharmacopeial Convention, Inc.: Rockville, MD, 2008; pp 2498–2499.
- (30) Glomme, A.; Marz, J.; Dressman, J. B. *J. Pharm. Sci.* **2005**, *94*, 1–16.
- (31) Kroner, M.; Schornick, G.; Feindt, H.; Meyer, T.; Ludwig, A.; Metzmann, U. U. S. Patent US5830985, November 3, 1998.
- (32) Kütt, A.; Leito, I.; Kaljurand, I.; Sooväli, L.; Vlasov, V. M.; Yagupolskii, L. M.; Koppel, I. A. *J. Org. Chem.* **2006**, *71*, 2829–2838.
- (33) Dossi, N.; Toniolo, R.; Susmel, S.; Pizzariello, A.; Bontempelli, G. *Chromatographia* **2006**, *63*, 557–562.
- (34) Cooke, C. L.; Davey, R. J. *Cryst. Growth Des.* **2008**, *8*, 3483–3485.
- (35) Serajuddin, A. T. M. *Adv. Drug Delivery Rev.* **2007**, *59*, 603–616.
- (36) Anderson, B. D.; Conradi, R. A. *J. Pharm. Sci.* **1985**, *74*, 815–820.
- (37) Galcera, J.; Molins, E. *Cryst. Growth Des.* **2009**, *9*, 327–334.
- (38) Lide, D. R., Ed. In *CRC Handbook of Chemistry and Physics, 89th Edition (Internet Version 2009): Aqueous Solubility and Henry's Law Constants of Organic Compounds, Section 8*; CRC Press/Taylor and Francis: Boca Raton, FL, 2009.
- (39) McKinnon, J. J.; Spackman, M. A.; Mitchell, A. S. *Acta Crystallogr., Sect. B* **2004**, *60*, 627–668.